Journal of Materials Chemistry C

Accepted Manuscript

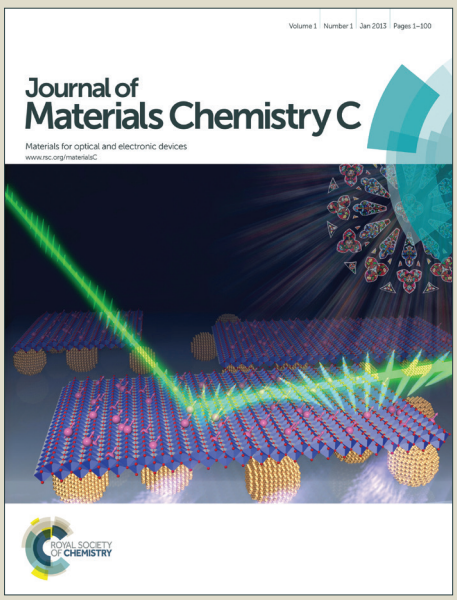

ROYAL SOCIETY OF CHEMISTRY

www.rsc.org/materialsC

Cite this: DOI: 10.1039/c0xx00000x

www.rsc.org/xxxxxx

Paper

Versatile displays based on 3-dimensionally ordered macroporous vanadium oxide film for advanced electrochromic device

Zhongqiu Tong[a], Haowei Yang[b], Li Na[b], Huiying Qu[b], Xiang Zhang[a], Jiupeng Zhao[b,], Yao Li[a,*]*

Received (in XXX, XXX) Xth XXXXXXXXX 20XX, Accepted Xth XXXXXXXXX 20XX

DOI: 10.1039/b000000x

3-dimensionally ordered macroporous (3DOM) vanadium oxide film was fabricated by anodic deposition of vanadium oxide into colloidal crystal template. The as-prepared films were investigated by X-ray diffraction (XRD), high resolution transmission electron microscopy (HRTEM), and X-ray photoelectron spectroscopy (XPS). The electrochemical and electrochromic behaviors of the films were studied in 1.0 M $LiClO_4$/propylene carbonate solution. Because of the larger surface area and shorter diffusion distance, the 3DOM film exhibited better electrochromic performance than the dense film prepared without template. The 3DOM film exhibited multicolor changes (yellow, green and black) in the voltage window from +1 to -1 V with a high transmittance modulation of *ca.* 34 % at 460 nm and high switching speed (1.5 s for coloration and 2.1 s for bleaching). Cyclic voltammetry (CV) and chronoamperometry measurements showed that the 3DOM structure is beneficial to the Li^+ diffusion in vanadium oxide films. A ITO/vanadia/gel/PEDOT:PSS/ITO electrochromic device was assembled, and the device showed multicolor changes with fast switching speed (3.5 s for anodic coloration and 3.4 s for cathodic coloration) and good cycling stability.

Introduction

Electrochromic (EC) materials are characterized by the ability to change their optical properties, reversible, and persistently, when a voltage is applied across them [1-3]. EC devices, especially "smart windows", have been attracting enormous attention during the last decades, because of not only their promising applications in indoor energy saving by controlling the solar light transmission indoors through reversible transmittance modulation, but also the comfortable esthetics accompanied the color changes [1-3]. Typically, a transition metal oxide film (e.g. WO_3, TiO_2, NiO, Co_2O_3, MoO_3) acts as the chromogenic electrode [4-9]. The reversible optical changes are caused by reversible electron-transfer reactions accompanied by electric-field-induced intercalation/de-intercalation of small ions (A^+) into/from a chromogenic oxide lattice (MO_y)[1-3].

$$MO_y + xA^+ + xe^- \leftrightarrow A_xMO_y \text{ (A: H, Li)} \quad (1)$$

(Bleached state) (Colored state)

The electroneutrality of the chromogenic electrode is maintained by simultaneous injection of ions and electrons. Thus, the chromatic contrast $\Delta T(\lambda)$ between bleached state and colored state is limited by the amount of accessible electroactive sites, while switching time τ is restricted by the ion penetration depths for achieving satisfactory color saturation [10-12]. Fabrication of nanostructured porous materials is a facile method to improve the electrochromic performance. Large surface significantly improves the chromatic contrast, while the short diffusion distance obviously accelerates the switching speeds [13-20].

Template synthesis is one of the most commonly used methods to fabricate porous electrochromic films because of its simplicity, versatility, and controllability. In recent years, three-dimensionally ordered macroporous (3DOM) films induced by self-assembled colloidal crystal template have been quickly developed due to interconnected porous network of nanometer thin walls and high surface-area-to-volume ratio [21-25]. Nanometer walls provide a short diffusion distance, ensuring the high switching speed; while high surface area provides enormous electroactive sites for redox reactions, leading to the large coloration modulation. Previous study has proved both the electron diffusion and ion diffusion behave as a 3D manner in 3DOM films, which can significantly accelerate the redox reactions during the electrochromic processes, leading to enhanced coloration contrast and improved switching response [25-27]. Furthermore, the bicontinuous structure provides continuous pore spaces for good electrolyte penetration[16-18].

Vanadium oxide has been studied extensively as a counter electrode material in electrochromic devices due to the ability of the vanadium ion to change its oxidation state as well as large amount of charge storage ability [10-12, 16, 17]. Moreover, as the only one oxide which is both anodic and cathodic coloration [28], vanadium oxide can demonstrate multicolor changes which leads to comfortable esthetics [29, 30]. However, the inherently low Li^+ diffusion coefficients (10^{-13} – 10^{-12} cm^2/s) and moderate electrical conductivity (10^{-3} – 10^{-2} S/cm) of vanadium oxide materials have limited their lithium ion intercalation properties [31, 32], leading to low coloration contrast and slow switching response in conventional flat films[14, 26]. A large surface area and a short diffusion distance are desired to achieve faster intercalation/extraction kinetics and more electroactive sites for redox reactions [11, 16-18].

In this work, a 3DOM vanadium oxide film was fabricated by anodic deposition of vanadium oxide into colloidal crystal template. Because of the larger surface area and shorter diffusion distance, the 3DOM film exhibited improved electrochromic performance (ΔT = 34 % at 460 nm, 1.5 s for coloration and 2.1 s for bleaching) compared with the dense film (ΔT = 16 % at 460 nm, 9.8 s for coloration and 11.5 s bleaching). Cyclic voltammetry (CV) and chronoamperometric measurements demonstrated the Li^+ chemical diffusion coefficient was significantly enhanced in the 3DOM nanostructure. An electrochromic device based on the 3DOM vanadium oxide film and spinning-coated poly (3, 4-ethylenedioxythiophene): polystyrenesulfonic acid (PEDOT:PSS) film was assembled. This electrochromic device exhibited multicolor changes with fast switching speed. Furthermore, after 150 cycles, no obvious transmittance modulation degradation was observed.

Experimental section

The monodispersed polystyrene (PS) spheres with 260 nm in diameter were obtained using emulsifier-free emulsion polymerization technology[27]. The self-assembly of monolayer PS sphere template was prepared as follows. Indium tin oxide (ITO) substrates (~9 Ω/cm^2, 1 cm × 3 cm) were ultrasonically cleaned in acetone, methanol, and distilled water for 20 min, respectively. The cleaned ITO glass substrates were placed into cylindrical vessels. PS sphere suspension diluted to 0.5 wt% was added into glass vessels and then evaporated in an incubator at a stable temperature of 60 °C.

Anodic deposition of vanadium oxide into polystyrene colloidal crystal templates was done as Ref. 27. Typically, 0.25 M $VOSO_4 \cdot 5H_2O$ in a 1:1 mixture (volume ratio) of distilled water and ethanol was used as electrolyte. The deposition voltage was 2 V versus Ag/AgCl and time was 35 s. After deposition, samples were immersed in a 1:1 mixture (volume ratio) of DMF and toluene for 24 h to remove the polystyrene templates. Finally, the as-prepared samples were dried at 130 °C for 5 h in vacuum to remove the absorbed solvent molecules. The as-prepared 3DOM vanadium oxide films showed a yellow-green color. For the sake of comparison, a dense vanadium oxide film was also prepared without template.

Spin-coating (3500 r/min) PEDOT: PSS films (EL-P 3040, AGFA) on ITO glass were used as counter electrodes for the assembly of the electrochromic devices. A lithium-based transparent and conductive gel electrolyte based on PMMA and $LiClO_4$ was prepared as follows. PMMA (6 g, Mw: 300,000) was dissolved in the dry acetonitrile (12 g), followed by adding 5 ml 1 M $LiClO_4$/propylene carbonate. Then, this viscous gel electrolyte was kept in the dark for 24 h before use. After the gel electrolyte was spread on the vanadium oxide-coated side of the electrodes, the two electrodes were placed in a position to make sure the polymer-coated sides face each other and then sandwiched. Finally, an epoxy resin was used to seal the device. This electrochromic device was marked as ITO/vanadia/gel/ PEDOT:PSS/ITO.

The morphologies of the 3DOM V_2O_5 films were characterized by scanning electron microscopy (SEM, FEI Helios Nanolab 600i). Crystalline structures of the V_2O_5 films were investigated by a rotation anode X-ray diffractometer (Japan Rigaku DMax-rb) with a graphite monochromatized Cu Kα radiation (0.15418 nm) and High Resolution Transmission Electron Microscope (HRTEM, FEI Tecnai G2F30, 300 kV). X-Ray photoelectron spectroscopy (XPS) study was conducted with a PHI 5700 ESCA System using Al Kα radiation (1486.6 eV). *In situ* visible and near-IR (NIR) electrochromic measurement was performed using an experimental setup produced in-house (same setup used in Ref. 27) in combination with a CHI 660C electrochemical workstation (Shanghai Chenhua Instrument Co. Ltd.). The experimental setup was sealed in an Argon-filled glove box (Vigor Glove Box from Suzhou, China) before testing. One side of the setup was connected to a white lamp (DT-mini-2-GS, Ocean Optics) by an optical fiber; the other side was connected to an optic spectrometer (MAYA 2000-Pro, Ocean Optics). The V_2O_5 film, Pt wire, and Ag/AgCl were used as a working electrode, a counter electrode, and a reference electrode, respectively. A 1 M solution of $LiClO_4$ in propylene carbonate was used as the electrolyte. The transmittance of the ITO glass in the electrolyte was used as a reference for 100 % transmittance. Before measuring the electrochromic performance of the V_2O_5 films, the film electrodes were subjected to three cyclic voltammetry (CV) cycles to ensure stability. CV measurements were performed at room temperature between +1 and −1 V at various scan rates. Chronoamperometric measurements were done by applying +1 V for 1000 s to de-intercalate all lithium ions present, then setting the potential back to 0.5 V or 0 V or -0.5 V for 500s, and monitoring the current as a function of time during testing.

Results and discussion

The preparation of the 3DOM vanadium oxide films is summarized schematically in Fig. 1a. The PS template presents good ordering close packed arrays with the average center-to-center distance of about 260 nm (Fig. 1b). Due to replication of the 3D ordered structures of the colloidal templates, vanadium oxide films grown directly on the conducting ITO layers display honeycomb structures with nanoscale walls throughout their entire volumes (Fig. 1c). The nanoscale walls can significantly decrease the diffusion length of Li^+ ions during electrochromic processes. Because of shrinkage during the removal of PS colloidal template, the macroporous structures become deformed. Two types of pores can be observed from the cross-section SEM image (Fig. 1d). The spaces belonged to PS spheres are transferred into large macropores, while the contact points between PS spheres are changed to small mesopores on the order of tens of nanometers. Such a hierarchical porous structure is expected not only to provide continuous voids for electrolyte penetration, but also to increase the number of possible intercalation sites. The thickness of 3DOM film obtained is about 1.7 μm. A dense film with a thickness of 550 nm was prepared for comparison (Fig. S1).

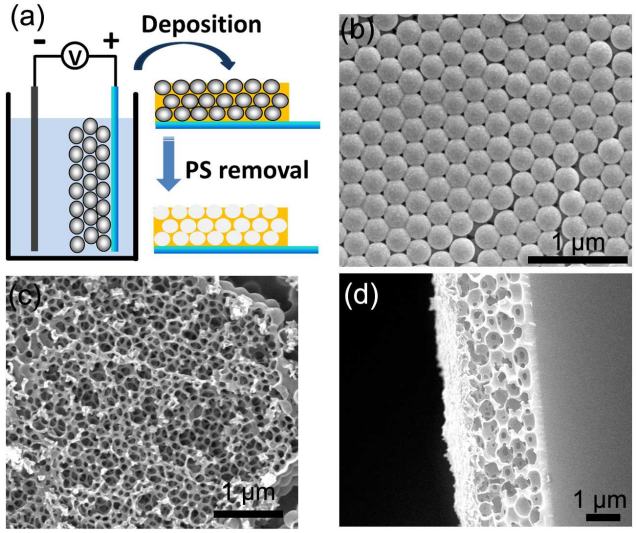

Fig. 1. (a) Schematic of preparation process for 3DOM vanadium oxide film. (b) Top-view SEM image of the PS colloidal template. (c) (d) Top-view and cross-section SEM images of 3DOM vanadium oxide film.

To investigate the 3DOM nanostructure, TEM and HRTEM examinations were performed. As shown in Fig. 2a, although the powerful ultrasonic treatment during the preparing TEM sample process has destroyed the nanostructure to some extent, 3DOM nanostructure is still clearly observed in the bright-field TEM image. Selected-area electron diffraction (SAED) pattern taken from the dashed circle area of this 3DOM nanostructure shows a weak contrast overlapping on the amorphous ring, as marked by an arrow in the inset of Fig. 2a. This indicates that some structural inhomogenities below the nanometer level exist. The arrow marked ring can be assigned to the (003) crystal planes of the $V_2O_5{\cdot}1.6H_2O$ nanocrystals. A HRTEM image of the 3DOM nanostructure is taken to further show the atom arrangement in the 3DOM walls (Fig. 2b). Consistent with the SAED pattern, traces of very tiny $V_2O_5{\cdot}1.6H_2O$ crystallites are found to be randomly presented in the glassy matrix. The size of these crystallites is below 2 nm as measured from the lattice fringes observed in the high resolution image. The observed lattice spacing is about 0.385 nm, which corresponds to the distance between the (003) crystal planes of the $V_2O_5{\cdot}1.6H_2O$ phase.

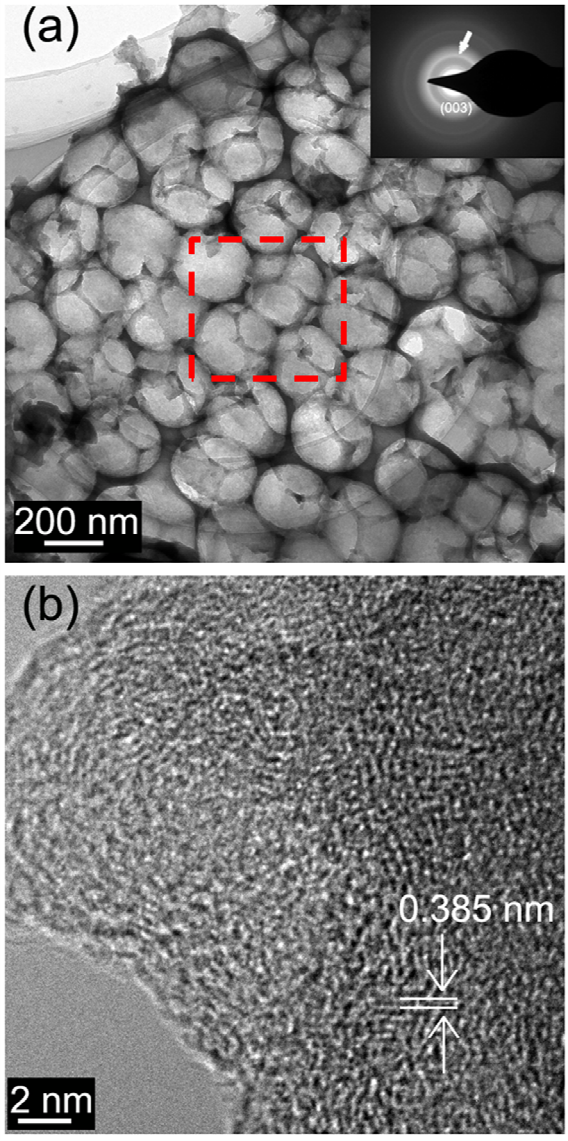

Fig. 2. (a) Bright-field TEM image of 3DOM vanadium oxide film. The inset SAED pattern is taken from the dashed circle area. (b) HRTEM image of the 3DOM wall.

X-ray diffraction pattern of the 3DOM vanadium oxide film is shown in Fig. 3a. In addition to the diffraction peaks of the ITO glass, no diffraction peaks of VO_x or $VO_x{\cdot}nH_2O$ are observed, indicating that the 3DOM network is amorphous. The diffraction peaks belonging to $V_2O_5{\cdot}1.6H_2O$ nanocrystallites are not observed in the XRD pattern. The reason may be that the amount of $V_2O_5{\cdot}1.6H_2O$ nanocrystallites is too small to be detected. Previous study has proved the dense film is also amorphous in nature [27]. Meanwhile, XPS was used to investigate the electronic structures and chemical bond information of the 3DOM vanadium oxide film. Fig. 3b shows the wide-range spectra of the obtained 3DOM vanadium oxide film. It is evident that only the photoelectrons of carbon, vanadium, tin and oxygen atoms are detected. The carbon is from the adsorbed organic solvents or carbonous molecules in air, while the tin is from the conducting ITO substrate. This wide-range XPS result indicates that the as-prepared vanadium oxide in 3DOM structure is rather

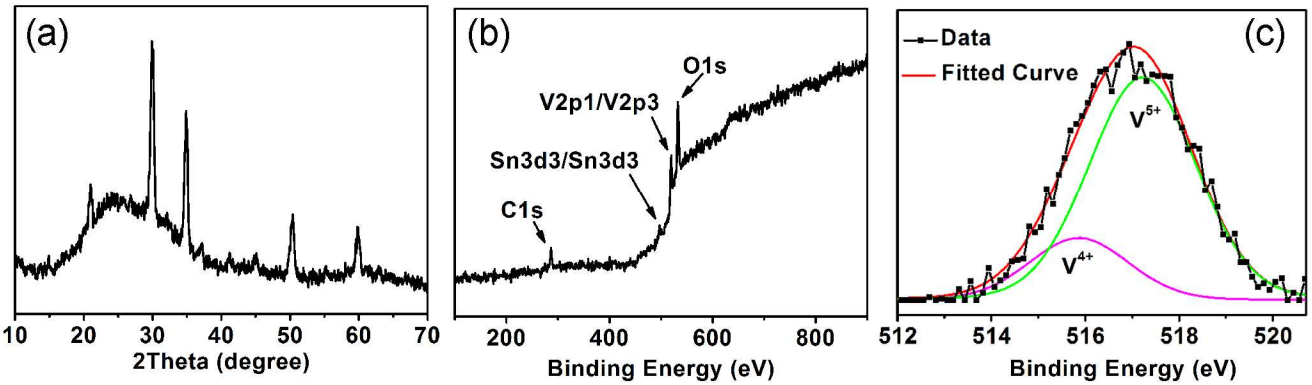

Fig. 3. (a) XRD pattern of 3DOM vanadium oxide film. (b) (c) Wide-range XPS data and V2p3/2 core peak spectra taken from 3DOM vanadium oxide film.

pure, and no impurity elements are detected. The $V2p_{3/2}$ core peak spectra for the as-prepared 3DOM film (Fig. 3c) is composed of two components located at 517.2 and 516.1 eV, respectively, as shown in the fitting data. These two binding energy values can be associated with two formal oxidation states, +5 and +4 [33, 34]. The ratio of V^{4+}/V^{5+} is 0.25, which is derived from the area ratio of the fitted spectrum of V $2p_{3/2}$ (V^{5+}) and V 2p3/2 (V^{4+}). V^{4+} ions in the as-prepared film may be derived from VO^{2+} ions in the solution. When the process of VO^{2+} anodic oxidation and deposition on ITO electrode occur, codeposition of unreacted VO^{2+} ions in the solution leads to the formation of V^{4+} in the as-prepared film. The existence of V^{4+} in the as-prepared 3DOM film corroborates the observed green-yellow color.

In situ visible and NIR transmittance measurements were used to investigate the electrochromic performance of the 3DOM vanadium oxide film and the dense film. Both the 3DOM film and the dense film were colored by applying a constant voltage of -1 V (*vs*. Ag/AgCl) for 40 s and bleached at 1 V (*vs*. Ag/AgCl) for 40 s. Fig. 4a shows the transmittance modulation (ΔT) of the 3DOM film, and the ΔT of the dense film is exhibited in Fig. S2a. Because of the larger surface area, the 3DOM vanadium oxide film provides more electroactive sites for intercalation/de-intercalation processes, leading to a higher ΔT than the dense film both in the visible and NIR spectrum ranges. At two typical wavelengths of 460 nm and 800 nm, the 3DOM film shows ΔT of *ca.* 35 % and 22 %, respectively. However, the dense film demonstrates only 16 % and 13 % at the above wavelengths. In the 3DOM nanostructured films, lithium intercalation into vanadium oxide under a cathodic potential of -1 V causes a fairly homogeneous transmission of *ca.* 60 % across the entire visible range, resulting in a black coloration (Fig. 4d). Charge extraction under an anodic potential of +1 V causes a strong absorption in the 400-500 nm spectral range, leading to a yellow color (Fig. 4d). Usually, the valence of vanadium ion in vanadium oxide film can be changed from +5 to +3 between -1 V and +1 V [10, 11], indicating different voltages leads to different amount mixture of V^{5+}, V^{4+} and V^{3+} ions, resulting in more than two color changes in the voltage window of ±1 V of the vanadium oxide film. Digital photos of the 3DOM film at 0.5 V, 0 V and -0.5 V are also exhibited in Fig. 4d. Two more colors can be obtained at 0.5 V (yellow with light green) and 0 V (green). The transmittance curve of the 3DOM film at 0 V is also shown in Fig. 4a.

Switching optical response under alternating potentials is another important evaluation factor of electrochromism. Alternating potentials lead to alternating intercalation/de-intercalation of Li^+ ions, resulting in coloration/bleaching switching [1, 2]. Switching behavior was analyzed by monitoring the transmittance at a wavelength of 460 nm under the application of a square wave voltage between +1 V and -1 V. Fig. 4b shows the transmittance-time response of the 3DOM film, and the response curve of the dense film is exhibited in Fig. S2b. The 3DOM film exhibits sharp changes during potential transitions, while the dense film shows gradual changes. This phenomenon clearly indicates that the 3DOM film has a much faster response than that of the dense film. When the switching time is defined as the time required to reach 90 % of a material's full transmittance change, the 3DOM film exhibits fast switching responses with 1.5 s for coloration and 2.1 s for bleaching, while the dense film shows 9.8 s for coloration and 11.5 s for bleaching. For the Li^+ ion intercalation/de-intercalation process, Li^+ ion diffusion distance x is equal to $(Dt)^{1/2}$, where D is the Li^+ ion chemical diffusion coefficient and t is the diffusion time [16]. In the 3DOM film, the thin walls provide much shorter diffusion distance than the dense film, resulting in much faster switching speed. Coloration efficiency (*CE*) is an important parameter for the evaluation of the optical modulation ability with energy consumption in the electrochromic materials [10, 11]. *CE* is defined as the ratio of change of optical density (ΔOD) at corresponding lithium ion insertion charge density (Q) per unit area (S), which is described as follows [10, 11]:

$$CE = \Delta OD/Q \quad (2)$$

$$\Delta OD = \log(T_b/T_c) \quad (3)$$

where T_b and T_c represent the transmittance of the bleached and colored sample, respectively. As shown in Fig. 4c, the 3DOM vanadium oxide film shows a high *CE* of *ca.* 42 $cm^2\ C^{-1}$ at the wavelength of 430 nm, because the high ΔT occurs in the spectrum range from 400 to 500 nm. The low ΔT in the remaining spectrum range leads to a rather low *CE* values, and an average *CE* of *ca.* 9.7 $cm^2\ C^{-1}$ is obtained in this spectrum range.

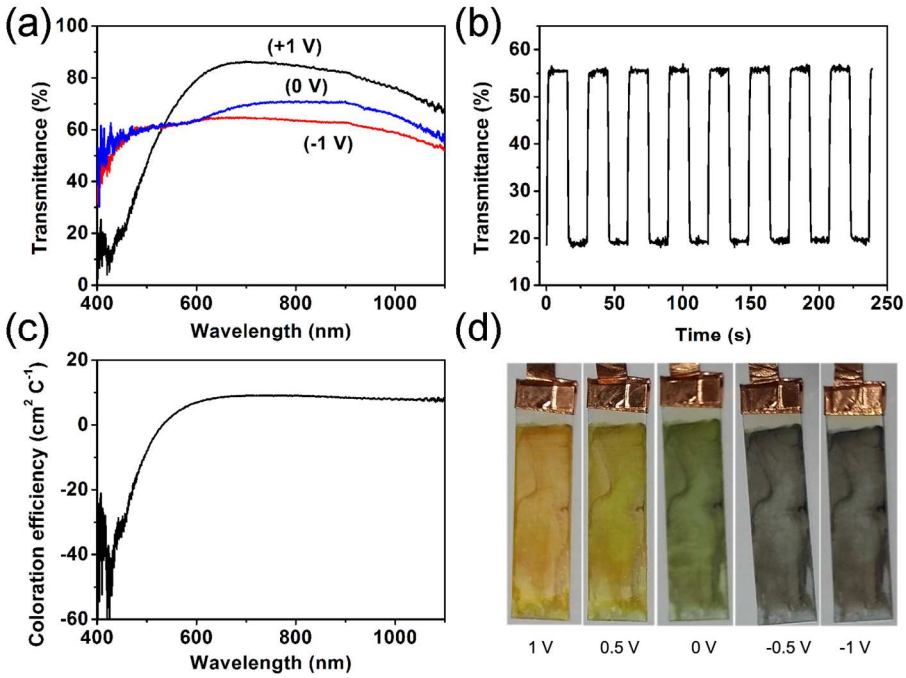

Fig. 4. (a) (b) (c) Transmittance contrast, transmittance-time switching response curve and coloration efficiency of 3DOM vanadium oxide film. (d) Electrochromic digital photographs of 3DOM vanadium oxide films under different potentials.

Cycling stability is another important aspect for the electrochromic materials. The transmittance modulations of the 3DOM film and the dense film at the 50th cycle are showed in Fig. S3a and S3b. The transmittance modulations at the 1st cycle are also showed for comparison. As shown in Fig. S3, the 3DOM film exhibits much higher cycling stability than that of the dense film. For the 3DOM film, no obvious changes are found for the transmittance curves both at coloration state (-1 V) and bleaching state (+1 V) after 49 cycles (Fig. S3a). In contrast, as for the dense film, although the transmittance curve at coloration state (-1 V) does not change after 49 cycles, the transmittance curve at bleaching state (+1 V) degrades apparently (Fig. S3b). The obvious degradation occurs in the spectrum range from 600 to 1100 nm, while small degradation is found in the remaining spectrum range.

The switching speed depends on the Li^+ diffusion distance (x) and Li^+ chemical diffusion coefficient (D). Moreover, previous studies have demonstrated the D varies much in different nanostructures [26, 27, 35]. It is reasonable to investigate the differences of D in the 3DOM nanostructure film and the dense film. Fig. 5a shows the CV curves of 3DOM vanadium oxide film at various scan rates. The featureless CV shape confirms the film is in amorphous nature. The reduction peaks shift to lower potentials, while the oxidation peaks move to the higher potentials with the increase of the scan rate. At low scan rates all the active surface areas can be utilized for the redox reactions, whereas at high scan rates, diffusion limits the movement of Li^+ ions due to the time constraint and only the outer active surface is utilized for the redox reactions. Thus the electrode polarization occurs and results in the shift of the redox peaks [26, 35]. The appearance of the redox peaks even at a high scan rate of 0.3 V s^{-1} indicates that the redox reactions in the 3DOM vanadium oxide film are reversible. For a simple solid state diffusion controlled process, the effective diffusion coefficient can be estimated from Randles-Servcik formula[26, 35, 36]:

$$i = 2.69 \times 10^5 \times A \times n^{2/3} \times D^{1/2} \times C_0 \times v^{1/2} \quad (4)$$

where i, D and v stand for the peak current, the effective diffusion coefficient, and the potential scan rate; A, n and C_0 represent the effective surface area of the electrode, the number of electrons transferred in a unit reaction, and the concentration of the diffusion species (Li^+ ions), respectively.

Fig. 5b shows the correlation between peak current i and square root of scan rate $v^{1/2}$. The perfect linear relationship reflects that the oxidation/reduction process of vanadium oxide in 3DOM film is controlled by the ion diffusion from the electrolyte to the electrode surface. However, as for the dense film (Fig. S4), the peak current deviates from the fitted curve, when the scan rate is above 0.1 V s^{-1}. This phenomenon indicates that the redox reactions in the dense film are much less reversible than those in the 3DOM film. Calculated from Eq. (4), the Li^+ ion chemical diffusion coefficients for the two kinds of films are shown in Table 1. The absolute value of the diffusion coefficients may not be accurate due to the limit of practical tests but we still could compare those values for further understanding the diffusion process in those films.) It is obvious that three-dimensional ordered structure is beneficial to the ion diffusion in vanadium oxide films. For the oxidation/coloration processes, the effective diffusion coefficients in the 3DOM films are improved up to ~5 times of those in the dense film.

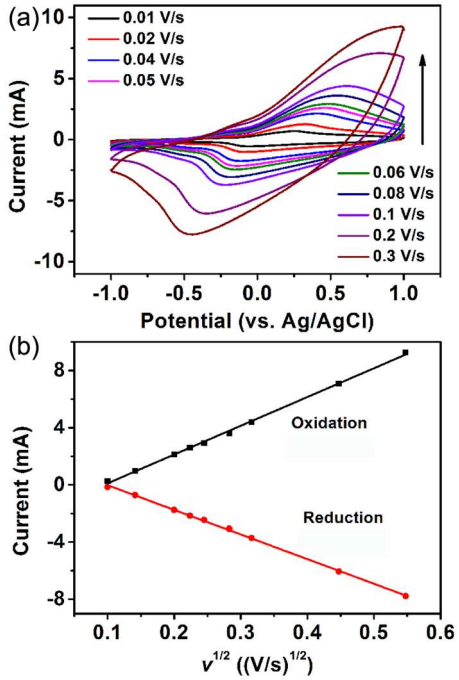

Fig. 5. (a) CV curves of the 3DOM vanadium oxide film at various scan rates. (b) Fitting plots between peak current *i* and square root of the scan rate $v^{1/2}$.

Table 1. Comparison of ion diffusion coefficients in 3DOM film and dense film with the data from references. Galvanostatic intermittent titration technique is short as GITT. Chronopotentiogram is short as CP.

	Sample	Measurement technique	Li^+ diffusion coefficient (cm^2/s)
Our work	3DOM film	CV	4.597×10^{-10} (Oxidation)
		CV	3.366×10^{-10} (Reduction)
		CA	1.093×10^{-9}(1 V to -0.5 V)
		CA	5.436×10^{-10} (1 V to 0 V)
		CA	1.722×10^{-10} (1 V to 0.5 V)
	Dense film	CV	8.934×10^{-11} (Oxidation)
		CV	7.792×10^{-11} (Reduction)
Ref. 39	$Li_xV_2O_{5-y}$ film	GITT	4×10^{-13} - 7×10^{-14}
Ref. 40	Dense film	GITT	1.1×10^{-11}
Ref. 41	Dense film	CP	3×10^{-12}

To be a strong complementary, the diffusion coefficients of the 3DOM vanadium oxide film were also tested using chronoamperometry (CA) technique. Chronoamperometry is a useful technology for the investigation of Li^+ diffusion coefficients in porous electrodes [37, 38]. Under the diffusion-limited conditions, the chronocoulometric response can be described by the following equation:

$$Q = 2n^{-1/2}FAD^{1/2}C_0t^{1/2} + Q_{dl} + nFA\Gamma \quad (5)$$

where Q is the integrated charge, A is the electrode area, D is the chemical diffusion coefficient, C_0 is the ion surface concentration, Q_{dl} is the double-layer charging, and Γ is the concentration of adsorbed species taking part in the faradic reaction. The chemical diffusion coefficients of the dense film are not investigated by using this electroanalysis technique, because Eq. (5) is based on the diffusion-limited conditions in nanoporous structure. Fig. 6a shows the chronoamperometric response curves of vanadium oxide film for the potential from +1 V to 0.5 V, 0 V and -0.5 V. The slopes obtained from the Q- $t^{1/2}$ plots of the intercalation and de-intercalation processes for the V_2O_5 films are plotted in Fig. 6b. The intercepts of these fit curves of the intercalation and de-intercalation processes in the 3DOM film are not equal to 0, indicating that the incorporation of 3DOM structure significantly impacts the behaviors of Li^+ diffusion. The slope is identified as $2n^{-1/2}FAD^{1/2}C_0$, according to Eq. (5). The calculated Li^+ ion chemical diffusion coefficients for the 3DOM film are shown in Table 1, and the Li^+ ion chemical diffusion coefficients of amorphous vanadium oxide from literatures are listed for comparison. For the 3DOM film, the Li^+ ion chemical diffusion coefficients detected by chronoamperometry technique are comparable with those data calculated from CV measurements, indicating the data from CV measurements are rather convincible. Compared with the data of the literatures, it can be further concluded the 3DOM structure improves the Li^+ ion chemical diffusion coefficients. The reasons may be due to two factors [16-18, 27, 42]: (1) because the vanadium oxide is in a 3DOM nanostructure, the double injection of ions and electrons during the redox reactions occurs in a 3D interconnected network. Such a facile ion and electron transport can significant accelerate the redox reactions; (2) the 3DOM structure provides enormous sharp edges, reducing the electrode polarization during the redox reactions, which can further accelerate the redox reactions.

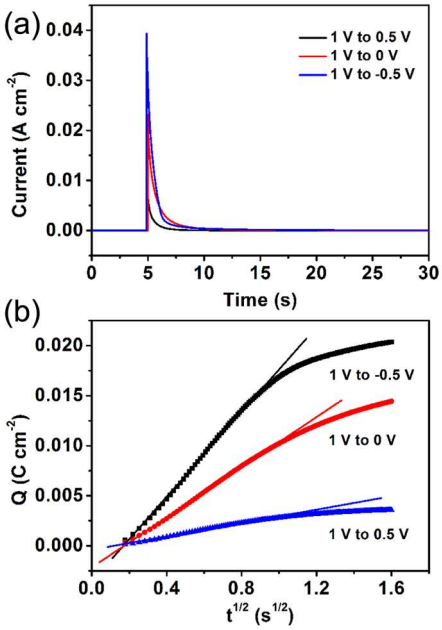

Fig. 6. (a) Chronoamperometric response curves of the 3DOM vanadium oxide film from +1 V to 0.5 V, 0 V and -0.5 V. (b) Fitting plots between inserted charge per area and square root of scan rate $t^{1/2}$.

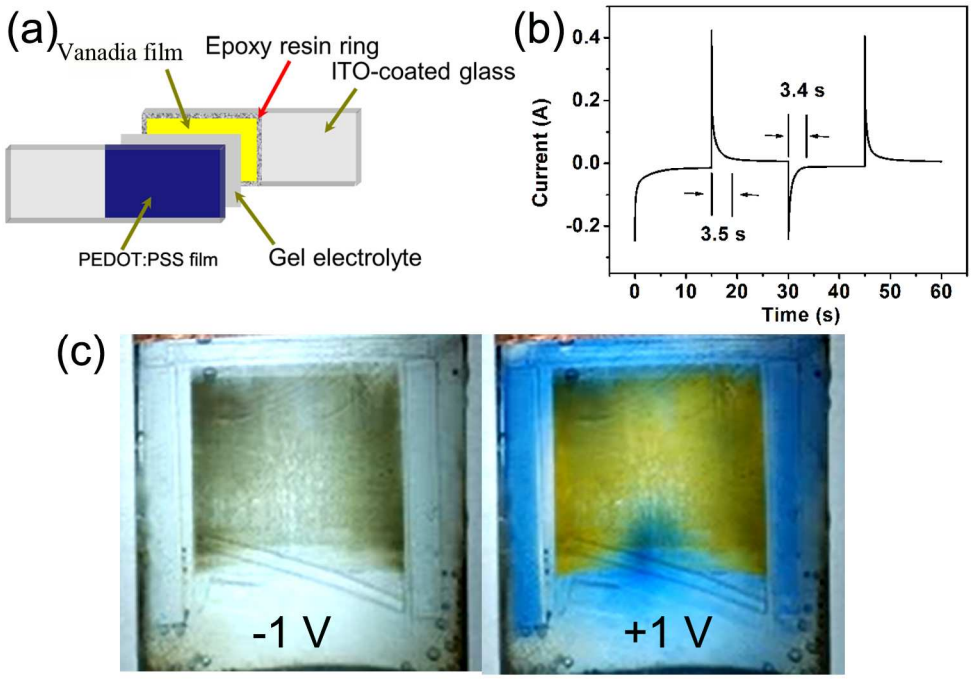

Fig. 7. (a) Schematic of electrochromic device based on the 3DOM vanadium oxide film and PEDOT:PSS film. (b) Transmittance-time switching response curve of the assembled electrochromic device. (c) Electrochromic digital photographs of the assembled electrochromic device under different potentials.

Finally, a sandwich structure of the electrochromic device based on the 3DOM vanadium oxide film and PEDOT:PSS film was fabricated by opponent-process theory (Fig. 7a). PEDOT is a cathodic coloration conducting polymer with blue color while transparent under positive polarization voltage. Thus when the vanadium oxide film exhibits yellow color under positive polarization voltage (+1 V), the PEDOT film exhibits the complementary color of blue. When the vanadium oxide film exhibits black color under negative polarization voltage (-1 V), the PEDOT film is in a transparent state. Fig. 7c shows the digital photos of the 3DOM vanadium oxide film based electrochromic device under positive voltage and negative voltage. The device also exhibits a rather fast switching speed with 3.5 s for anodic coloration and 3.4 s for cathodic coloration (Fig. 7b). A video showing the electrochromic response of the assembled device during the alternating voltages is provided in the Supporting Information.

To further compare the electrochromic performance of 3DOM film with the dense film, an electrochromic device based on vanadium oxide dense film was also fabricated. Fig. S5a and S5b shows the transmittance modulations of the electrochromic devices fabricated with 3DOM vanadium oxide film and dense vanadium oxide film at 1st cycle and 150th cycle. Because the device-assembling is based on the opponent-process theory, the transmittance-modulation curves of the devices are similar to those of the vanadium oxide film (Fig. 4a). The maximum transmittance modulation occurs in the wavelength range from 400 to 600 nm, which is consistent with the color changes during the alternating voltages (yellow to brownish black), as shown in Fig. 7c. Due to the large surface area and short diffusion distance, the device fabricated with the 3DOM film shows higher transmittance modulation and cycling stability than those of the device fabricated with dense vanadium oxide film. The device fabricated with the 3DOM film exhibits *ca.* 23 % at 460 nm, while the device fabricated with dense film demonstrates only *ca.* 8.1 % at the same wavelength. Furthermore, after 150 cycles, no obvious transmittance modulation degradation is observed in the device fabricated with 3DOM film, while for the device fabricated with dense film, transmittance modulation degradation of 50 % is observed at 460 nm.

Conclusions

Three-dimensionally ordered macroporous (3DOM) vanadium oxide film was successfully fabricated through anodic deposition with colloidal crystal templates. XRD and HRTEM examinations show the vanadium oxide is in amorphous nature, while XPS data demonstrate that the vanadium ions have two kinds of valence states (V^{4+} and V^{5+}). Because of the larger surface area and shorter diffusion distance, the 3DOM film exhibits better electrochromic performance than the dense film. The 3DOM film exhibits multicolor changes (yellow, green and black) in the voltage window from +1 to -1 V with a high transmittance modulation of *ca.* 34 % at 460 nm and high switching speed (1.5 s for coloration and 2.1 s for bleaching). Li^+ ion chemical diffusion coefficient examinations present that the 3DOM structure is beneficial to the ion diffusion in vanadium oxide films. Finally, an electrochromic device based on 3DOM vanadium oxide film and PEDOT:PSS film is assembled. The device shows multicolor changes with fast switching speed (3.5 s for anodic coloration and 3.4 s for cathodic coloration). This device also exhibits high cycling stability. After 150 cycles, no obvious transmittance modulation degradation is observed.

Acknowledgements

We thank National Natural Science Foundation of China (no. 510 10005, 91216123, 51174063), Natural Science Funds for Distinguished Young Scholar of Heilongjiang province, The Natural Science Foundation of Heilongjiang Province (E201436), the International Science & Technology Cooperation Program of China (2013DFR10630) and Specialized Research Fund for the Doctoral Program of Higher Education (SRFDP 20132302110031).

Notes and references

‡

[a] *Center for Composite Material, Harbin Institute of Technology, Harbin, China. Fax: 086 45186402345; Tel: 086 451 86402345; E-mail: yaoli@hit.edu.cn*

[b] *School of Chemical Engineering and Technology , Harbin Institute of Technology, 150001, Harbin, China. E-mail: jpzhao@hit.edu.cn*

1 D. R. Rosseinsky and R. J. Mortimer, *Adv. Mater.*, 2001, **13**, 783-793.

2 V. K. Thakur, G. Q. Ding, J. Ma, P. S. Lee and X. H. Lu, *Adv. Mater.*, **2012**, *24*, 4071-4096.

3 E. S. Lee, S. E. Selkowitz, R. D. Clear, D. L. DiBartolomeo, J. H. Klems, L. L. Fernandes, G. J. Ward, V. Inkarojrit and M. Yazdanian, California Energy Commission, PIER, 2006 CEC-500-2006-052.

4 M. Layani, P. Darmawan, W. L. Foo, L. Liu, A. Kamyshny, D. Mandler, S. Magdassi and P. S. Lee, *Nanoscale*, 2014, **6**, 4572-4576.

5 S. Berger, A. Ghicov, Y.-C. Nah, and P. Schmuki, *Langmuir*, 2009, **25**, 4841-4844.

6 G.-F. Cai, J.-P. Tu, J. Zhang, Y.-J. Mai, Y. Lu, C.-D. Gu and X.-L. Wang, *Nanoscale*, 2012, 4, 5724-5730.

7 X. H. Xia, J. P. Tu, J. Zhang, J. Y. Xiang, X. L. Wang and X. B. Zhao, *ACS Appl. Mater. Interfaces*, 2010, **2**, 186-192.

8 J. M. Wang, E. Khoo, P. S. Lee and J. Ma, *J. Phys. Chem. C*, 2008, **112**, 14306-14312.

9 L. Zhang, Y. Xu, D. Jin and Y. Xie, *Chem. Mater.*, 2009, **21**, 5681-5690.

10 Y. Wang and G. Z. Cao, *Chem. Mater.*, 2006, **18**, 2787-2804.

11 Y. Wang, K. Takahashi, K. Lee and G. Z. Cao, *Adv. Funct. Mater.*, 2006, **16**, 1133-1144.

12 Y. Yang, D. Kim and P. Schmuki, *Electrochem. Commun*., 2011, **13**, 1021-1025.

13 K. Lee, D. Kim, S. Berger, R. Kirchgeorg and P. Schmuki, *J. Mater. Chem.*, 2012, 22, 9821-9825.

14 K. Takahashi, Y. Wang and G. Z. Cao, *Appl. Phys. Lett.*, 2005, **86**, 053102.

15 J. Zhang, J.-P. Tu, D. Zhang, Y.-Q. Qiao, X.-H. Xia, X.-L. Wang and C.-D. Gu, *J. Mater. Chem.*, 2011, **21**, 17316-17324.

16 M. R. J. Scherer, L. Li, P. M. S. Cunha, O. A. Scherman and U. Steiner, *Adv. Mater.*, 2012, **24**, 1217-1221.

17 D. Wei, M. R. J. Scherer, C. Bower, P. Andrew, T. Ryhanen and U. Steiner, Nano Lett., 2012, 12, 1857-1862.

18 M. R. J. Scherer and U. steiner, *Nano Lett.*, 2013, **13**, 3005-3010.

19 X. H. Xia, J. P. Tu, J. Zhang, J. Y. Xiang, X. L. Wang and X. B. Zhao, *Sol. Energy Mater. Sol. Cells*, 2010, **94**, 386-389.

20 W. B. Kang, C. Y. Yan, X. Wang, C. Y. Foo, A. W. M. Tan, K. J. Z. Chee and P. S. Lee, *J. Mater. Chem. C*, 2014, 2, 4727-4732.

21 Y. Xia, B. Gates, Y. Yin and Y. Lu, *Adv. Mater.*, 2000, **12**, 693-713.

22 A. Stein, F. Li and N. R. Denny, *Chem. Mater.*, 2008, **20**, 649-666.

23 A. Stein, B. E. Wilson and S. G. Rudisill, *Chem. Soc. Rev.*, 2013, **42**, 2763-2803.

24 F. Li, D. P. Josephson and A. Stein, *Angew. Chem. Int. Ed.*, 2011, **50**, 360 -388.

25 X. H. Xia, J. P. Tu, J. Zhang, X. H. Huang, X. L. Wang, X. B. Zhao, *Electrochim. Acta*, 2010, **55**, 989-994.

26 D. T. Ge, L. L. Yang, Z. Q. Tong, Y. B. Ding, W. H. Xin, J. P. Zhao and Y. Li, *Electrochim. Acta*, 2013, 104, 191-197.

27 Z. Q. Tong, J. Hao, K. Zhang, J. P. Zhao, B.-L. Su and Yao Li, *J. Mater. Chem. C*, 2014, 2, 3651-3658.

28 C. G. Granqvist, *Sol. Energy Mater. Sol. Cells*, 2012, **99**, 1-13.

29 Y. X. Lu, L. Liu, D. Mandler and P. S. Lee, J. Mater. Chem. C, 2013, 1, 7380-7386.

30 Y. Yang, D. Kim, P. Schmuki, *Electrochem. Commun*., 2011, **13**, 1198-1201.

31 E. Portiron, A. L. Salle, A. Varbaere, Y. Piffard, and D. Guyomard, *Electrochim. Acta*, 1999, **45**, 197-214.

32 J. M. McGraw, C. S. Bahn, P. A. Parilla, J. D. Perkins, D. W. Readey and D.S. Ginley, *Electrochim.Acta*, 1999, **45**, 187-196.

33 G. Silversmit, D. Depla, H. Poelman, G. B. Marin and R. D. Gryse, *J. Electron Spectrosc. Relat. Phenom.*, 2004, **135**, 167-175.

34 J. Mendialdua, R. Casanova and Y. Barbaux, *J. Electron Spectrosc. Relat. Phenom.*, 1995, **71**, 249-261.

35 J.-G. Zhang, E. C. Tracy, D. K. Benson and S. K. Deb, *J. Mater. Res.*, 1993, 8, 2649-2656.

36 R. Sivakumar, A. M. E. Raj, B. Subramanian, M. Jayachandran, D. C. Trivendi and C. Sanjeeviraja, *Mater. Res. Bull.*, 2004, **39**, 1479-1489.

37 H. Lindstrom, S. Sodergren, A. Solbrand, H. Rensmo, J. Hjelm, A. Hagfeldt and S.-E. Lindquist, *J. Phys. Chem. B*, 1997, **101**, 7710-7716.

38 J. Liu and A. Manthiram, *J. Electrochem. Soc.*, 2009, **156**, A833-A838.

39 S. Lee, J. Eom and H. Kwon, *J. Appl. Electrochem.*, 2009, **39**, 241–245.

40 J. Scarminio, P. R. Catarini, A. Urbano, R. V. Gelamo, F. P. Rouxinol and M. A. Bica de Moraes, *J. Braz. Chem. Soc.*, 2008, 19, 788-794.

41 K. Le Van, H. Groult, A. Mantoux, L. Perrigaud, F. Lantelme, R. Lindström, R. Badour-Hadjean, S. Zanna and D. Lincot, *J. Power Sources*, 2006, 160, 592-601.

42 L. L. Yang, D. T. Ge, J. P. Zhao, Y. B. Ding, X. P. Kong and Y. Li, *Sol. Energy Mater. Sol. Cells*, 2012, **100**, 251-257.

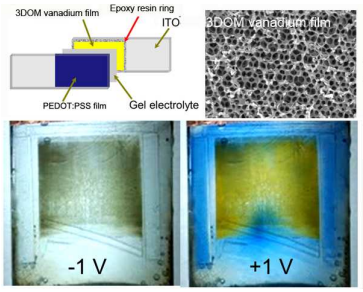

An electrochromic device based on 3DOM vanadium oxide film and PEDOT:PSS film is fabricated, and this device shows multicolor changes with fast switching speed and good cycling stability.